JOURNAL OF GEOPHYSICAL RESEARCH, VOL. 108, NO. B8, 2359, doi:10.1029/2002JB002108, 2003

Thermal diffusivity of upper mantle rocks: Influence of temperature, pressure, and the deformation fabric

Benoit Gibert
Laboratoire de Tectonophysique, Université Montpellier II and CNRS, Montpellier, France

Ulfert Seipold
GeoForschungsZentrum Potsdam, Potsdam, Germany

Andréa Tommasi and David Mainprice
Laboratoire de Tectonophysique, Université Montpellier II and CNRS, Montpellier, France

Received 19 July 2002; revised 19 February 2003; accepted 1 April 2003; published 1 August 2003.

[1] Thermal diffusivity measurements of seven naturally deformed upper mantle rocks were made as a function of pressure (up to 1 GPa), temperature (up to 1250 K), and the deformation fabric of the samples. For each sample the strain-induced crystal preferred orientations of olivine and pyroxenes were measured, and petrophysical models, based on the thermal diffusivity tensors of the olivine and enstatite crystals, were used to evaluate the three-dimensional distribution of the thermal diffusivity. Both model predictions and measurements show that the anisotropy of thermal diffusivity remains large at the rock scale: 15–28%, depending on the strength of the olivine crystallographic fabric. The direction of maximum thermal diffusivity is parallel to the lineation (flow direction), and the minimum of thermal diffusivity is normal to the foliation plane (flow plane). This anisotropy is preserved at high temperature and pressure. However, measured thermal diffusivities are 20–30% lower than model predictions. This discrepancy between measurements and model predictions cannot be explained by the presence of cracks in the samples because the closure of these void spaces, evaluated through the high-pressure experiments, is found to have a negligible effect on measured thermal diffusivities. Thermal diffusivity for all samples displays a weak linear dependence on pressure of $\sim$10% GPa^{-1}. Thermal diffusivities observed in the high-temperature experiments (1000–1250 K) are compatible with a weak radiative contribution to the total heat diffusion. *INDEX TERMS:* 5112 Physical Properties of Rocks: Microstructure; 5134 Physical Properties of Rocks: Thermal properties; 8120 Tectonophysics: Dynamics of lithosphere and mantle—general; 8130 Tectonophysics: Heat generation and transport; *KEYWORDS:* mantle rocks, thermal diffusivity, lattice diffusivity, radiative heat transfer, anisotropy, petrophysical models.

Citation: Gibert, B., U. Seipold, A. Tommasi, and D. Mainprice, Thermal diffusivity of upper mantle rocks: Influence of temperature, pressure, and the deformation fabric, *J. Geophys. Res.*, *108*(B8), 2359, doi:10.1029/2002JB002108, 2003.

1. Introduction

[2] Heat transfer is a key process for the upper mantle dynamics. In the lithosphere, heat transfer by conduction is expected to be the main process leading to thermal equilibrium. Thermal diffusivity is thus the key parameter that controls the temperature distribution as a function of time and, indirectly, through the temperature dependence of the rheology, the deformation pattern in the lithospheric mantle. Knowledge of pressure and temperature derivatives of thermal diffusivity of mantle materials is therefore essential to model the thermal evolution of the lithosphere. Thermal diffusivity of mantle rocks is known to decrease strongly with increasing temperature up to 1000 K. At higher temperatures, it is supposed to either remain constant up to 1600 K [*Katsura*, 1995] or to increase due to an increasing contribution of radiative processes [*Kanamori et al.*, 1968]. Pressure dependence is expected to be low [*Katsura*, 1995]. At last, thermal diffusivity of olivine and pyroxene crystals is anisotropic [*Chai et al.*, 1996; *Kobayashi*, 1974].

[3] However, a close analysis of thermal diffusivity (and conductivity) data for mantle materials highlights a large scatter of the proposed thermal diffusivity values, depending on the experimental settings and on the type of sample used, that is, single crystals, sintered aggregates or natural rocks. Indeed, thermal diffusivity of single crystals and polymineralic rocks differs widely at ambient conditions [*Beck et al.*, 1978; *Horai and Susaki*, 1989; *Kanamori et al.*, 1968]. Thermal diffusivity data at high-temperature conditions, in which radiative heat transport becomes impor-

0148-0227/03/2002JB002108$09.00

Table 1. Samples Origin, Modal Composition, Densities, and the Mean Forsterite Content of Olivine[a]

Sample	Peridotite Type	Origin	Modal Composition,%				Density, kg m^{-3}	Mg/(Fe+Mg), %
			ol	en	di	sp		
BALM4	lherzolite	Balmuccia massif, Alps	76	19	3	2	3363	90
BALD1	lherzolites	Baldissero massif, Alps	75	18	5	2	3354	90
00BA1		Baldissero massif, Alps					3383	90
00BA2		Baldissero massif, Alps					3354	90
PNG	harzburgite	Papua New Guinea-ophiolitic nappe	87	12	0	1	3330	91.1
00VS11	dunitic lens within gabbros	Balmuccia massif	98	–	–	2	3429	84.2
00VS24	dunites	Balmuccia massif	98	–	–	2	3387	90.5

[a]Modal compositions (ol, olivine; en, enstatite; di, diopside; and sp, spinel) were calculated by image analysis performed on thin sections. Chemical analyses were performed on a CAMECA SX100 electron probe microanalyzer at the Institut des Sciences de la Terre, de l'Eau et de l'Espace de Montpellier.

tant, also exhibit a similar discrepancy between single-crystal and polycrystal behavior [*Kanamori et al.*, 1968; *Katsura*, 1995; *Schatz and Simmons*, 1972]. This discrepancy is also observed in high-pressure experiments, in which the effect of void spaces in the polycrystalline material is minimized [*Horai and Susaki*, 1989; *Zaug et al.*, 1992].

[4] The additional effects expected in polycrystalline rocks, compared to single crystals, are (1) presence of cracks or open porosity, which should lower absolute values of thermal diffusivity and modify the anisotropy, (2) grain boundaries, which may reduce the thermal diffusivity through dispersion processes, (3) variations in modal composition of rocks, as well as in the chemical composition of the constitutive minerals, and (4) deformation, which induces the development of crystal preferred orientations and thus anisotropy of thermal diffusivity at the rock scale [*Kobayashi*, 1974; *Tommasi et al.*, 2001].

[5] The association of petrophysical simulations and measurements of thermal diffusivity of natural rock samples allows to establish a link between single-crystal and rock properties (i.e., polycrystalline aggregates) [*Pribnow and Umsonst*, 1993; *Siegesmund*, 1994]. For instance, in a recent study, we have shown that up to one half of the strong thermal diffusivity anisotropy of the olivine single crystal may be preserved at the rock scale [*Tommasi et al.*, 2001].

[6] In this paper, we continue the investigation of heat transfer properties of upper mantle rocks. Thermal diffusivity of seven peridotites was measured under high-temperature (up to 1250K) and high-pressure conditions (up to 1 GPa). Whole rock thermal diffusivities were also modeled using the olivine and pyroxenes single-crystal tensors. The comparison between measurements, model predictions, and previous thermal diffusivity data allows a discussion of the physical processes affecting the upper mantle thermal diffusivity under a large range of pressure and temperature conditions.

2. Sample Description

2.1. Microstructure

[7] Seven naturally deformed mantle rocks have been selected for both petrophysical modeling and laboratory measurements of thermal diffusivity. Four spinel lherzolites were chosen as representative of a subcontinental mantle. A harzburgite was selected as representative of the suboceanic mantle and two dunites were chosen as almost pure olivine end-member samples. Apart from the harzburgite, which has been sampled in the Papua New Guinea Ophiolite, all the other samples come from the Ivrea Zone, Italy. Origin of the samples, their modal composition, densities, and the forsterite content of olivine in each sample are shown in Table 1.

[8] Optical observations on thin sections (Figure 1a) show that all samples are devoid of alteration minerals and macroscopic fractures. Densities measured by triple-weight method in dry and saturated conditions are close to those calculated using olivine pyroxenes and spinel single-crystal densities and are thus incompatible with presence of serpentine (Table 1). Connected porosity measured on 3–4 cm^3 samples is inferior to 0.2%; this confirms that open macrofractures are absent. Preferred orientations of intergranular or intragranular cracks are not observed on thin sections.

[9] All samples show a clear foliation and lineation defined by alignment of elongated spinels. Except for one dunite (00VS11), all samples display coarse-grained porphyroclastic textures characteristic of deformation under high temperature conditions (>1000°C). Olivine displays a bimodal grain size distribution: porphyroclasts range from 2 to 5 mm whereas recrystallized grains are smaller than 1 mm. In the lherzolites and harzburgite, orthopyroxenes form clusters that may reach up to 5 mm in diameter (Figure 1b). In the lherzolites, olivine grains are slightly elongated parallel to the lineation direction indicated by the stretching of spinel grains (Figure 1b). In the harzburgite PNG and the dunite 00VS24, intense recrystallization by subgrain rotation leads to elongation of olivine porphyroclasts normal to the spinel lineation. In the dunite 00VS11, olivine grains display a polygonal structure, with typical 120° triple junctions and spinel inclusions in olivine, which are indicative of static recrystallization at high temperature.

2.2. Crystal Preferred Orientations

[10] Crystal preferred orientations (CPO) of olivine and pyroxenes grains were determined by the electron-backscattered diffraction (EBSD) technique in a JEOL 5600 scanning electron microscope. Diffraction patterns (Kikuchi bands), generated by the interaction of a vertical electron beam with a carefully polished thin section tilted to 70°, are automatically indexed by the CHANNEL+ software from HKL Technology. For each measured grain, the full crystallographic orientation is given by the three Euler angles (φ_1, Φ, φ_2) that describe the rotation needed to bring the macroscopic and crystallographic reference frames into

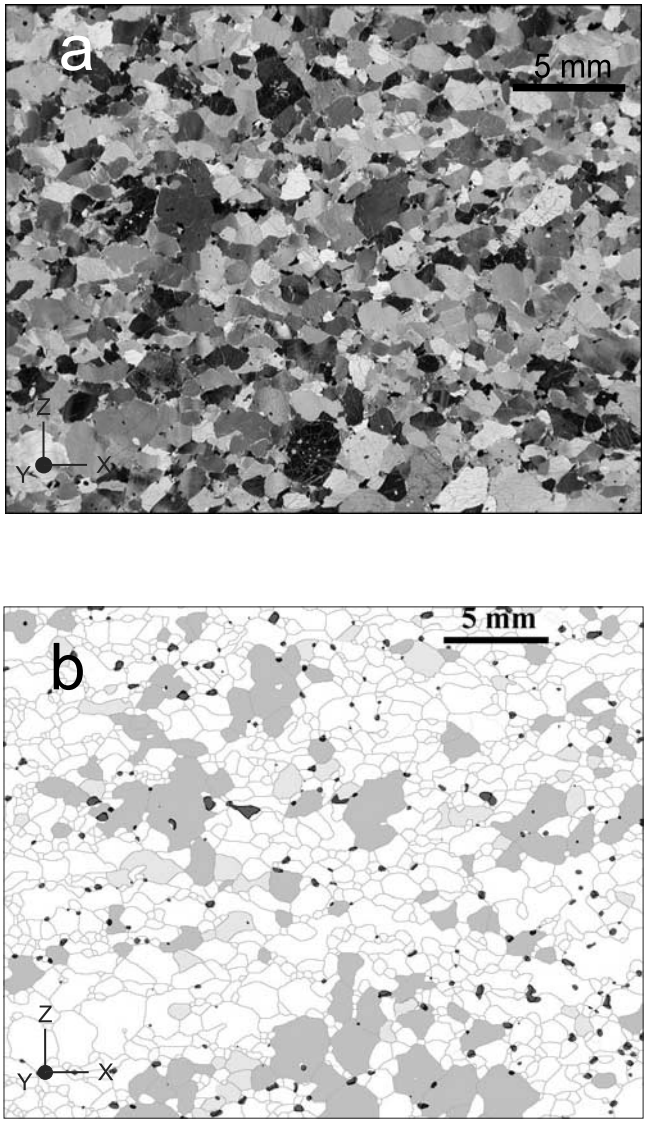

Figure 1. Microstructure of the lherzolite sample BALM4. The *X* direction is the lineation direction and the (*XY*) plane is the foliation plane. (a) Thin-section micrograph with crossed polarizers. (b) Line drawing. Spinels are represented in black, orthopyroxenes are in dark grey, clinopyroxenes are in light grey, and olivine is in white.

coincidence [*Bunge*, 1982]. Measured crystals preferred orientations (Figure 2) are typical of peridotites deformed under high temperature conditions (>1000°C). BALD1, PNG, 00BA1, and 00BA2 display a strong concentration of olivine [100] axes subparallel to the lineation (*X* direction, density >8) and a girdle distribution of [010] and [001] axes in the plane perpendicular to the lineation. Within this girdle, a maximum of the [010] axes is observed perpendicular to the foliation plane (*Z* direction) and a secondary maximum is observed in the foliation plane (normal to the lineation) for 00BA2 and BALD1 (*Y* direction). [001] maxima, usually weaker than the [100] and [010] ones, are observed normal to the lineation, in the foliation plane (*Y* direction). This CPO pattern suggests a dominant activation of the high-temperature (010)[100] and (001)[100] slip systems. BALM4 displays a planar distribution of the [100] and [001] along the foliation plane and a strong concentration of the [010] axes normal to foliation. This olivine CPO pattern is characteristic of a flattening deformation (axial shortening or transpression, [*Tommasi et al.*, 1999]). The dunites, 00VS24 and 00VS11, show an olivine CPO with an orthorhombic symmetry, characterized by equivalent concentrations (maximum density ≅ 5 multiples of uniform distribution) of the [100], [010], and [001] axes in the *X*, *Z,* and *Y* directions, respectively. This CPO pattern is characteristic of single activation of the olivine high-temperature easy-glide system: (010)[100], probably associated with an active grain boundary migration (also indicated by the microstructure of these dunites).

[11] Enstatite CPO are, in general, well correlated with the olivine ones. The [001] axes tend to concentrate parallel or at low angle to both the spinel lineation and the [100] maximum of olivine, suggesting dominant glide parallel to the easy glide direction of orthopyroxenes [001]. A strong obliquity between the olivine and enstatite CPO is nevertheless observed for BALD1 and 00BA2, suggesting either dominant glide on the unusual (001)[010] slip system or a weaker deformation of the pyroxenes relative to the olivine matrix. Diopside crystal preferred orientations are very weak.

3. Modeling the Thermal Diffusivity at the Sample Scale

[12] If the modal composition and the crystallographic orientations of a rock sample (polycrystalline aggregate) are known, the three-dimensional distribution of its thermal diffusivity may be calculated using the thermal diffusivity tensors of the constitutive phases [*Mainprice and Humbert*, 1994]. In the present models, we use olivine and enstatite single-crystal thermal diffusivity tensors (Table 2) determined by picosecond transient grating spectroscopy [*Chai et al.*, 1996]. The full thermal diffusivity tensor of monoclinic diopside is unknown, but measurements parallel to the [100], [010], and [001] directions indicate that it is similar to the enstatite one [*Kobayashi*, 1974], so in the present models diopside is assimilated to enstatite. The aggregate thermal diffusivity is obtained by averaging the individual grain tensors in the macroscopic reference frame (*XYZ* structural directions). Each mineral phase is pondered by its volume fraction. Two kinds of averaging are used. The Voigt average is obtained by assuming that the thermal gradient is constant everywhere and equal to the macroscopic thermal gradient. The Reuss average is obtained by assuming that heat flux is everywhere constant. The Voigt average is an upper bound for thermal diffusivity estimation and the Reuss average is a lower bound [*Taylor*, 1983]. For our samples, because the diffusivity of olivine and pyroxenes are similar, these two bounds were very close. Thus we used their arithmetic mean: the Voigt-Reuss-Hill average.

[13] These petrophysical models (Figure 2) show that all samples display a significant anisotropy of thermal diffusivity (between 17.5 and 29.8%). Thermal diffusivity is maximum parallel to the olivine [100] concentration, i.e., parallel to the *X* direction, and minimum parallel to the olivine [010] axes concentration, i.e., perpendicular to the foliation plane (*Z* direction). The good agreement between the aggregates

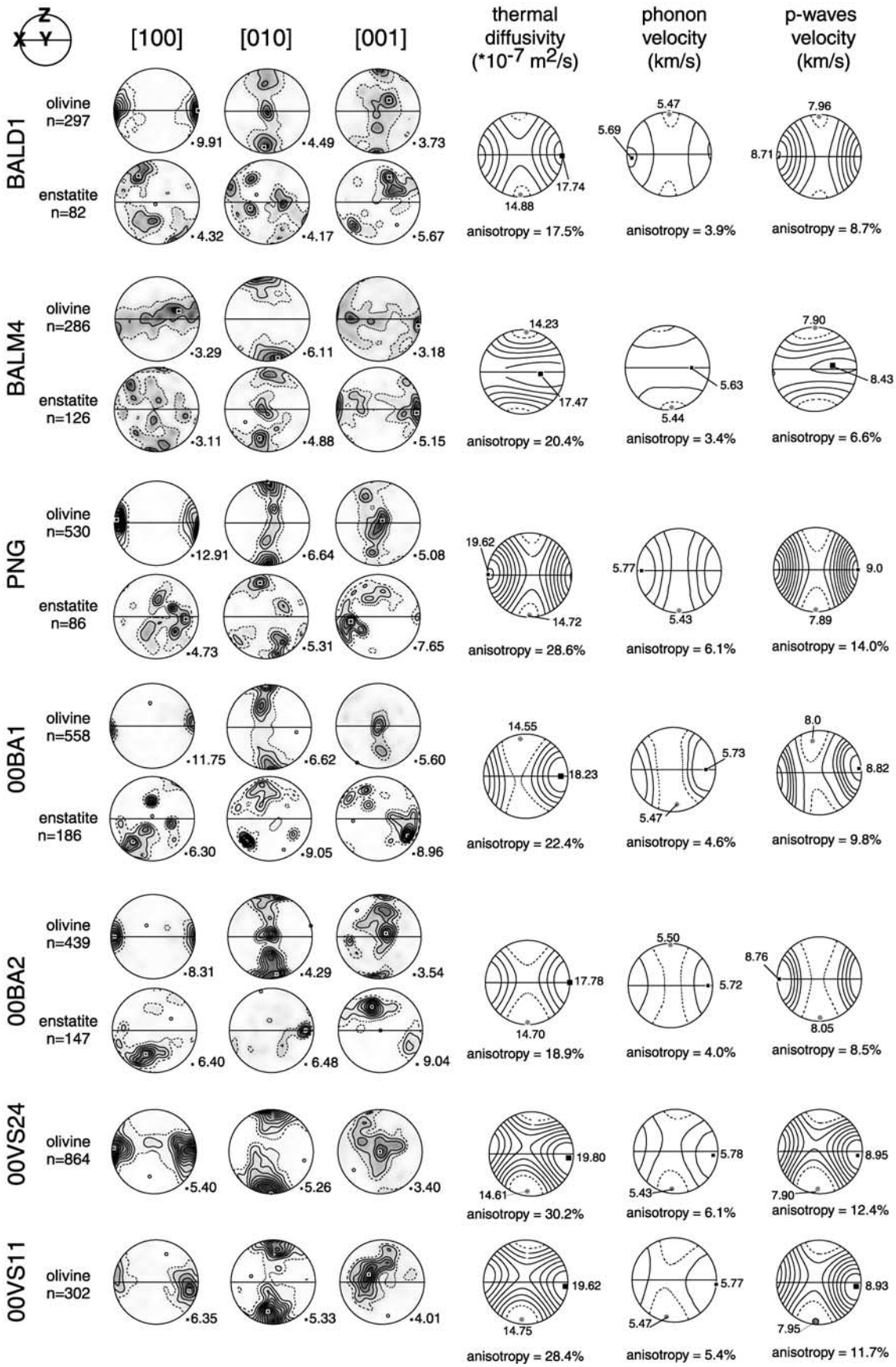
Z
X Y
[100]
[010]
[001]
thermal diffusivity (*10-7 m2/s)
phonon velocity (km/s)
p-waves velocity (km/s)
BALD1
olivine n=297
9.91
4.49
3.73
enstatite n=82
4.32
4.17
5.67
17.74
14.88
anisotropy = 17.5%
5.47
5.69
anisotropy = 3.9%
7.96
8.71
anisotropy = 8.7%
BALM4
olivine n=286
3.29
6.11
3.18
enstatite n=126
3.11
4.88
5.15
14.23
17.47
anisotropy = 20.4%
5.63
5.44
anisotropy = 3.4%
7.90
8.43
anisotropy = 6.6%
PNG
olivine n=530
12.91
6.64
5.08
enstatite n=86
4.73
5.31
7.65
19.62
14.72
anisotropy = 28.6%
5.77
5.43
anisotropy = 6.1%
9.0
7.89
anisotropy = 14.0%
00BA1
olivine n=558
11.75
6.62
5.60
enstatite n=186
6.30
9.05
8.96
14.55
18.23
anisotropy = 22.4%
5.73
5.47
anisotropy = 4.6%
8.0
8.82
anisotropy = 9.8%
00BA2
olivine n=439
8.31
4.29
3.54
enstatite n=147
6.40
6.48
9.04
17.78
14.70
anisotropy = 18.9%
5.50
5.72
anisotropy = 4.0%
8.76
8.05
anisotropy = 8.5%
00VS24
olivine n=864
5.40
5.26
3.40
19.80
14.61
anisotropy = 30.2%
5.78
5.43
anisotropy = 6.1%
8.95
7.90
anisotropy = 12.4%
00VS11
olivine n=302
6.35
5.33
4.01
19.62
14.75
anisotropy = 28.4%
5.77
5.47
anisotropy = 5.4%
8.93
7.95
anisotropy = 11.7%

Table 2. San Carlos Olivine (Fo89) and Orthopyroxene Thermal Diffusivity Tensors[a]

Axis	Olivine	Orthopyroxene
[100]	21.6	12.6
[010]	12.5	10.5
[001]	18.7	16.6

[a]From [*Chai et al.*, 1996]. In units of 10^{-7} m^2 s^{-1}. Since olivine and orthopyroxene are orthorhombic minerals, thermal diffusivity measurements along the three principal crystallographic axes define the complete tensor. Maximum anisotropy for olivine is 54%.

and the olivine crystal thermal diffusivity tensors indicates that the three-dimensional distribution of thermal diffusivity at the rock scale is essentially controlled by the olivine crystal preferred orientation. However, the anisotropy depends not only on the strength of the olivine [100] axes concentration but also on the relative distribution of the [010] and [001] axes. In samples where the minimum diffusivity direction [010] and the intermediate direction [001] display a girdle distribution in the plane normal to the lineation (*YZ* plane), the anisotropy is weakened (e.g., BALD1 and 00BA2). In contrast, samples in which the [010] axes are strongly concentrated display a strong anisotropy (e.g., BALM4). Thermal diffusivity anisotropy depends also on pyroxene content. High pyroxene contents tend to weaken the anisotropy, even if the highest diffusive axis of pyroxenes, [001], is concentrated close to the highest diffusive axis of olivine. This effect is present for 00BA1, which displays the strongest olivine CPO, but a low anisotropy (22%). In comparison, the 00VS24 and 00VS11 dunites display a weaker CPO, but higher anisotropy (≅30%), because of their orthorhombic symmetry. Absolute values of thermal diffusivity are also strongly dependent on the pyroxene content of the samples because pyroxenes are less diffusive than olivine: the dunites and the harzburgite display higher thermal diffusivities than the lherzolites.

[14] In order to constrain the thermal diffusivity modeling, we have also calculated the *P* wave velocity distribution for our samples using elastic constants tensors of olivine and enstatite determined at ambient conditions [*Abramson et al.*, 1997; *Duffy and Vaughan*, 1988]. Comparison between the calculated thermal diffusivities and *P* wave velocities highlights a clear relationship between acoustic properties and thermal properties (Figure 2). The direction of maximum *P* wave velocity, which is parallel to the flow direction (*X* direction), is also the most diffusive direction and the direction of minimum *P* wave velocity corresponds to the less diffusive direction. Since the anisotropy intensity for both *P* wave propagation and thermal diffusivity depends directly on the olivine CPO, the samples with greatest anisotropy for the acoustic properties have also the greatest anisotropy for the thermal diffusivity. Thus a link exists between deformation of mantle rocks as probed by measurements of the anisotropy of seismic velocities (e.g., *Pn* anisotropy, *SKS* splitting) and anisotropy of thermal diffusivity. However, for all samples, the *P* wave velocity anisotropy is significantly lower than the thermal diffusivity anisotropy.

[15] In conclusion, petrophysical modeling suggests that, under ambient conditions, upper mantle rocks retain one third to one half of the anisotropy of thermal diffusivity of the olivine single crystal, depending on the strength of olivine crystallographic fabric and pyroxenes content. Heat diffusion is the fastest parallel to the direction of the olivine [100] concentration, i.e., parallel to the flow direction, and slowest perpendicular to the foliation plane. However, these models only consider the effect of the crystallographic orientation of the constituent phases on the whole rock thermal diffusivity. To investigate the influence of other parameters, such as heat dispersion at grain boundaries, crystalline imperfections, or microcracks, as well as the effect of pressure and temperature, on thermal diffusivity, we measured the thermal diffusivity of these rocks under increasing temperature (ambient pressure, up to 1000°C), and increasing pressure (ambient temperature, up to 1 GPa). For each sample, we evaluated the anisotropy of thermal diffusivity by measuring the thermal diffusivity parallel to the lineation (*X* direction, in which the highest diffusivity is expected), normal to foliation (*Z* direction, the lowest diffusivity direction) and, in some samples, normal to the lineation within the foliation plane (along the *Y* direction).

4. Thermal Diffusivity Measurements

4.1. Method and Errors Considerations

[16] A finite pulse method in cylindrical geometry is used to determine thermal diffusivity of rock cores with 27 mm in diameter and 43 mm length [*Seipold*, 1988]. A pulse of 3 s in duration and energy of ~80 J is generated at the core axis by means of a Nichrome heater of 0.2 mm diameter. It propagates radially and is recorded by a chromel-alumel thermocouple placed at a distance *d* of 7mm from the core axis. The temperature response is measured every 0.1 s during 70 s. The temperature evolution is fitted by a polynomial function from which the half-time value t_H the time span to reach half of the maximum temperature rise, is evaluated. Thermal diffusivity *D* is then determined using equation (1) [*Seipold*, 1988, equation 7], which is derived from the theoretical description of the radial propagation of a zero-length heat pulse in an infinite cylindrical sample [*Carslaw and Jaeger*, 1959]:

$$D = \frac{d^2}{10.77 t_H - 16.55}. \quad (1)$$

Figure 2. (opposite) Olivine and enstatite crystal preferred orientations and calculated three-dimensional thermal diffusivity, phonon velocity, and *P* wave velocity distributions for each sample. Lower hemisphere stereographic projections. Solid lines mark the foliation (*XY* plane), and the lineation (*X* direction) is horizontal. In the crystal preferred orientation stereoplots, *n* represents the number of measured grains, contours intervals are at 0.5 multiples of a uniform distribution, and inverse log shading varies from white (minimum density) to black (maximum density indicated by the solid square). Thermal diffusivity plots are contoured at 0.5×10^{-7} m^2 s^{-1} intervals. Phonon and *P* wave velocities are contoured at 0.1 km s^{-1} intervals. Anisotropy is defined by $(D_{max}-D_{min})/D_{mean}$ in %.

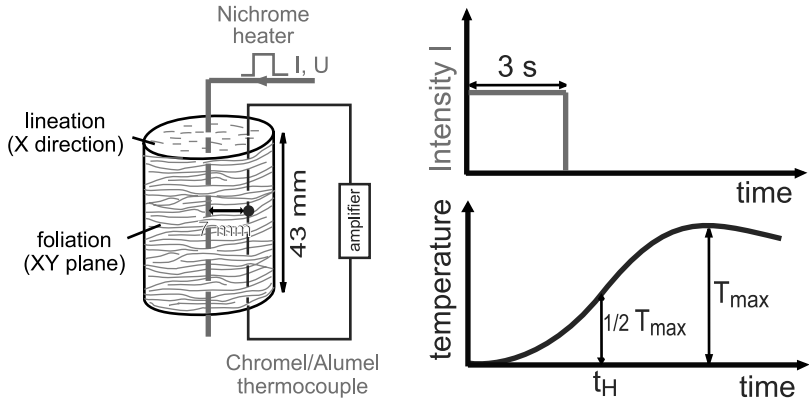

Figure 3. Scheme of the transient method used to measure thermal diffusivity of rocks as a function of the structural direction (the *X* direction in this case).

Since heat transfer takes place essentially radially from the core axis, this method is well adapted for the measurement of the thermal diffusivity in an anisotropic medium (Figure 3). In order to determine the three eigenvalues of the thermal diffusivity tensor, we used at least three cores for each sample and varied the coring direction and the position of thermocouple so that in each core the direction heat wire–thermocouple is parallel to one of the main axes of structural reference frame (*X*, *Y*, or *Z*).

[17] In high-temperature measurements, a thick-walled Macor container surrounds the sample in order to prevent a drastic step in thermal properties at the sample boundary and thermal convection. It also limits the generation of cracks through the sample at high temperatures. A three-zone furnace ensures a homogeneous temperature within the sample. High-pressure experiments were conducted in an oil pressure device, which insures perfectly hydrostatic conditions. Sample and oil are placed in a high-pressure vessel with an inner diameter of 40.5 mm. A sheet of elastic polyurethane covers the sample surface in order to prevent the penetration of the silicon oil (pressure medium).

[18] Transient thermal diffusivity measurements, like the one we used in this study, are submitted to several kinds of uncertainties. The most important one results from an inaccuracy in the evaluation of the distance between heater and thermocouple, *d*, because thermal diffusivity is proportional to the square of this distance (equation (1)). In our device, the position of the heater is known with an accuracy of less than 0.1 mm. Thus *d* depends on the position, the size and the type of thermocouple (sheathed or not). In high-temperature experiments, in which sheathed thermocouples of 0.2 mm in diameter were used, the position of thermocouple is known with an uncertainty of $\sim$0.1 mm, which lead to an error of 1.5% on *d* and of 3% on the thermal diffusivity measurement. In high-pressure experiments, hand-made thermocouples were used. This results in an additional error source, because the junction between the chromel and alumel wires may not be exactly in contact with the rock, leading to a systematic underestimation of the thermal diffusivity. Analyses of the cores at the end of the experiments show that the distance between the rock and the thermocouple is generally lower than 0.2 mm, which in average leads to a systematic underestimation of the thermal diffusivity 6%. However, it is important to note that the uncertainty in the determination of the heater-thermocouple distance is independent of temperature or pressure and does not affect temperature or pressure derivatives. Effects of thermal expansion [*Bouhifd et al.*, 1996] and compressibility [*Abramson et al.*, 1997] on the heater-thermocouple distance are found to be negligible.

[19] Uncertainties due to the electronic noise, data acquisition, as well as errors due to failure to reach thermal equilibrium within the sample, are more difficult to quantify. In order to evaluate this uncertainty, at each temperature or pressure step we performed at least three successive measurements, spaced by five minutes in order to return to thermal equilibrium within the sample. Scatter of these three measurements gives a good estimation of this uncertainty. Finally, when it was possible, two series of measurements with different cores were conducted in each direction, in order to test data reproducibility and the representativity of the measurement.

4.2. Thermal Cracking

[20] At ambient conditions, the present method has been thoroughly tested using standard materials like Macor and Pyroceram. In addition, thermal diffusivity data on rocks have been tested by comparison with measurements performed at the Geophysical Survey of Finland [*Kukkonen et al.*, 1999]. However, at high temperature/ambient pressure conditions, thermally induced cracks caused by mismatches in thermal expansivities between neighboring crystals (e.g., anisotropic thermal expansion in olivine grains of different orientations) may artificially lower the thermal transport properties of the rock sample. Thus, in absence of experiments at both high-pressure/high-temperature conditions, the absolute accuracy of the present measurements at high temperature is an unproven assertion, and the high-temperature measurements may underestimate the upper mantle thermal diffusivity.

[21] However, the reproducibility of the measurements in successive high-temperature experiments as well as a careful examination of the observed temperature dependence of the thermal diffusivity and anisotropy provide some indirect evidence, discussed below, that thermal cracking has not substantially affected the present high-temperature measurements. In addition, we use a two-step measuring procedure that should allow a rough estimate of the effect of thermally

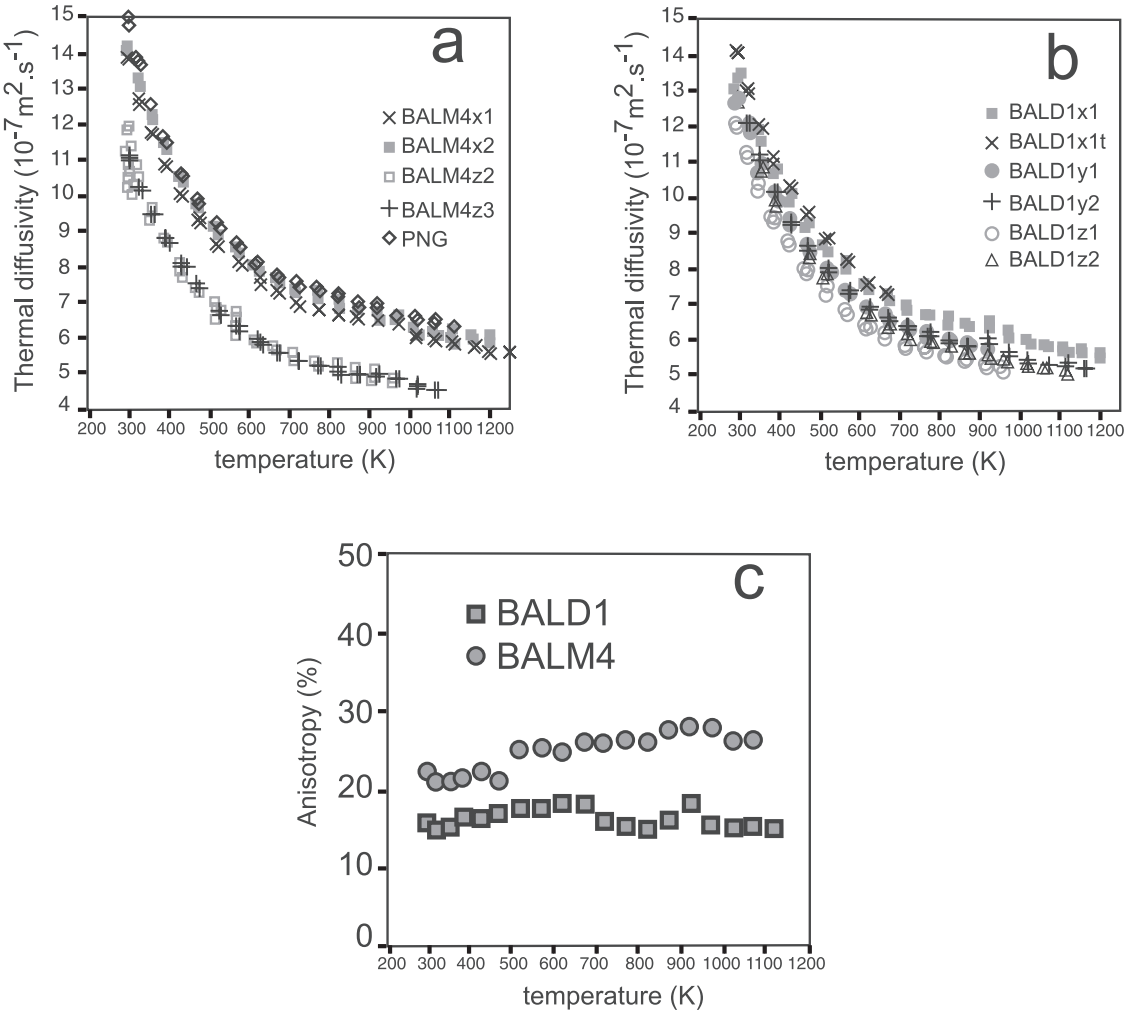

Figure 4. Thermal diffusivity as a function of temperature for (a) BALM4 (in the *X* and *Z* directions of the structural reference frame) and PNG (in the *X* direction) and for (b) BALD1 (in the *X*, *Y,* and *Z* directions). (c) Anisotropy of thermal diffusivity as a function of temperature for samples BALM4 and BALD1.

induced cracks on the measured thermal diffusivities. The thermal diffusivity is measured in a first run-up to 850–950 K. Then the temperature is lowered to ambient conditions and a second run is performed up to the maximum temperature (1100–1250 K). In the present experiments, it was always observed that, although the measured diffusivities at ambient conditions are lower than in the first run, at the final temperature of the first run the measured thermal diffusivities vary by <3%. This systematic observation suggests that under increasing temperature conditions, thermally induced cracks probably remain closed and hence do not affect significantly the thermal transport properties of rocks [*Seipold*, 1998].

4.3. Results

[22] Thermal diffusivity of eleven cores from three samples: two lherzolites (BALM4 and BALD1) and one harzburgite (PNG), has been measured under ambient pressure and temperatures ranging from 290K and 1250 K (Figure 4). A full evaluation of the thermal diffusivity tensor (measurements in the *X*, *Y,* and *Z* direction) has only been possible for BALD1. Lack of material limited the investigation of BALM4 to measurements in the maximum and minimum diffusivity directions (*X* and *Z*, respectively) and of PNG to the *X* direction. The weak scatter of the successive measurements at each temperature step as well as of the reproducibility tests indicates that errors due to electronic noise or thermal disequilibria are low (<1%). The reproducibility of thermal diffusivity measurements in a given direction for different samples is indirect evidence that thermal cracking does not affect substantially the high-temperature measurements, since this process should vary from sample to sample.

[23] Analysis of this data set highlights that thermal diffusivity of mantle rocks is anisotropic. Heat diffusion is the fastest parallel to the lineation (*X* direction) and the slowest normal to the foliation (*Z* direction) under the entire studied temperature range. Maximum and minimum thermal diffusivities are consistent from sample to sample. Moreover, all samples, independent on the measurement direction, display a similar temperature dependence: a strong decrease of thermal diffusivity up to 500–600 K

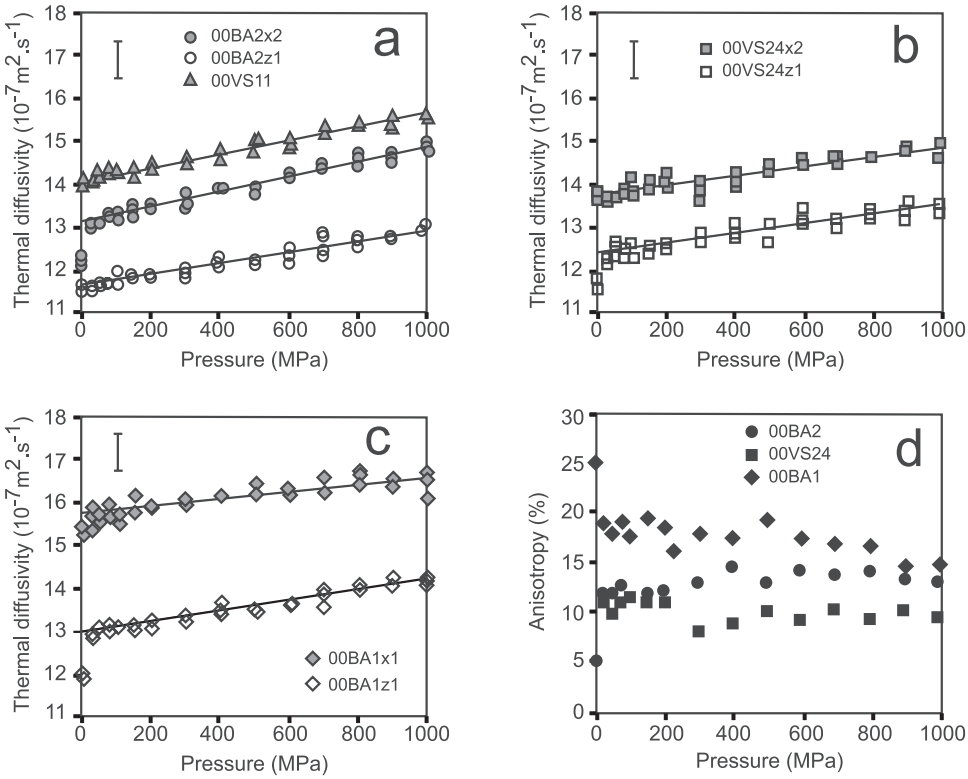

Figure 5. Thermal diffusivity measured as a function of pressure for (a) 00BA2 and 00VS11, (b) 00VS24, and (c) 00BA1. For each curve, the linear fit is shown. Error bars due to uncertainty on the thermocouple position are of 6%. (d) Anisotropy of thermal diffusivity as a function of pressure for 00BA2, 00VS24, and 00BA1.

that is followed by a slower decrease up to 1250 K. The weak decrease of thermal diffusivity in the high temperature range suggests that thermal cracking does not affects significantly the high-temperature measurements, since optical analysis of samples issued from high- and low-temperature experiments shows that this process is most active up temperatures higher than 600 K. Thermal diffusivity anisotropy increases slightly at high temperature (Figure 4c). It is stronger for BALM4 (25%) than for BALD1 (17%).

[24] Thermal diffusivity measurements under ambient temperature and pressures varying from 0 to 1 GPa have been performed on two lherzolites (00BA1 and 00BA2) and two dunites (00VS24 and 00VS11). Except for 00VS11, only measured in the X direction, two different cores have been used for measurements of the thermal diffusivity parallel to the X and to the Z directions (Figure 5). These measurements clearly show (1) a preservation of the thermal diffusivity anisotropy up to 1000 MPa and (2) a weak linear dependence on pressure between 25 and 1000 MPa.

[25] The higher scatter of the three successive measurements performed at each pressure step highlights the higher uncertainty of the high-pressure data compared to the high-temperature results. This scatter is always higher at ambient temperature (even in the high-temperature device), when thermal diffusivity is maximum and thermal equilibrium is more difficult to achieve. However, the higher scatter of this data is also due to the inherent difficulty of the high-pressure work (delicate electrical connections, etc.). Finally, as discussed on the previous section, an imperfect contact between the sample and the hand-made thermocouples used in the high-pressure measurement may also lead to underestimation of thermal diffusivity. Indeed, the weak (<10%) nonlinear increase of thermal diffusivity observed for same samples (00BA1Z1, 00BA2X1, and 00VS24Z1) between 0 and 25 MPa may be due to a bad contact between rock and thermocouple at low pressure. The higher uncertainty of these high-pressure data may also explain the slightly different anisotropy variation (Figure 5d) as a function of pressure from sample to sample: the anisotropy remains constant for 00VS24, increases for OOBA2, and decreases for 00BA1. Absolute values of thermal diffusivity follow the following trend: $D_{00BA1x} > D_{00VS24x} > D_{00BA2x}$ and $D_{00BA1z} > D_{OOVS24z} > D_{OOBA2z}$.

5. Comparison Between Thermal Diffusivities Predicted by Petrophysical Modeling and Measured Values

[26] Analysis of the present thermal diffusivity data in the light of the petrophysical modeling predictions clearly shows that the thermal diffusivity anisotropy of upper mantle rocks is controlled by the olivine crystals preferred orientation. Thermal diffusivity anisotropy estimated from measurements in the high-temperature device is in good agreement with model predictions. Thermal diffusivity anisotropy is stronger for BALM4 than for BALD1. More-

Table 3. Previous Measurements of Thermal Diffusivity (or Conductivity) of Mantle Materials at Ambient Conditions

Sample	Method	Thermal Diffusivity, 10^{-7} m^2 s^{-1}	Ref[a]
Horoman dunite (oriented)	angstrom (linear)	*X* direction 18.5	1
	angstrom (linear)	*Y* direction 14.7	1
		Z direction 13.6	
Lherzolithe 12	hot wire (transient) uncertainty 6%	9.5	2
Lherzolithe 4	hot wire (transient)	12.3	2
Olivine powder Fo91	needle probe method	18.1	4
Carolina dunite 1		13.0 (273 K)	3
Musckox dunite	hot wire (steady)	17.4 (273 K)	3
Single crystal 1	uncertainty unknown	20.2 (273 K)	3
Single crystal 2		33.4 (273 K)	3
Olivine single crystals Fo91.6	angstrom (linear) uncertainty of 5–0%	[100] axis 21.8	1
Olivine single crystals Fo91.6		[010] axis 10.7	1
Olivine single crystals Fo91.6		[001] axis 17.1	1
Olivine single crystal Fo82	angstrom (linear) uncertainty 5–10%	[001] axis 18.5	(5)

[a]References: 1, *Kobayashi* [1974]; 2, *Horai and Susaki* [1989]; 3, *Beck et al.* [1978]; 4, *Horai* [1971]; and 5, *Kanamori et al.* [1968].

over, PNG, whose thermal diffusivity was only measured in the *X* direction displays the highest diffusivity; indeed its olivine CPO is the strongest. In fact, in these experiments, maximum and minimum thermal diffusivities are consistent from sample to sample, and their relative magnitude also matches model predictions: $D_{PNG} > D_{BALM4X} = D_{BALD1X} > D_{BALDY} > D_{BALD1Z} > D_{BALM4X}$.

[27] In high-pressure experiments, the relationship of model-measurements is less clear. For instance, although the dunite 00VS24 was expected to have a higher diffusivity than the lherzolite 00BA1, experiments show the contrary. In addition, measured anisotropy for 00VS24 is much lower than the predicted values (Figure 5d). The higher uncertainties in the high-pressure experiments may explain this disagreement between model and observations. Another explanation may invoke the short distance heater-thermocouple (7 mm) relative to the mean grain size (0.5 mm); the measurements sample only 10–20 grains, while the models integrate between 300 and 800 grains. Thus it is possible that a measurement may not be exactly representative of the measured crystallographic fabric and modal composition, especially for samples whose CPO is not very strong, like 00VS24, or whose grain size is large, like the dunites. However, the high-temperature experiments, for which two series of measurements were conducted on two different cores of the same direction, show a good reproducibility (Figure 4).

[28] In spite of the relatively good agreement between model and measurements, measured thermal diffusivity under ambient conditions is lower than model predictions by ~20–30%. Open microfractures may hinder heat transfer (or seismic wave propagation) and thus explain such a difference between the modeled physical property and its measurement on a real rock. Closure of these air-filled cracks is known to lead to a nonlinear increase of thermal diffusivity between 0 and 50–100 MPa [*Durham et al.*, 1987; *Horai and Susaki*, 1989; *Seipold et al.*, 1998]. However, in the present high-pressure data, this nonlinear increase is absent or very weak (Figure 5); the slightly nonlinear increase in thermal diffusivity between 0 and 25 MPa observed on some measurements is probably due to a bad contact between the thermocouple and the sample. Connected porosity measured on our samples is very low (<0.3%), suggesting that open cracks are probably absent. In consequence, the discrepancy between measurements and models cannot be explained by open microfractures. Two other reasons may be invoked to explain this discrepancy. First, the thermal diffusivity tensors given by *Chai et al.* [1996] may overestimate the actual olivine thermal diffusivity. Second, grain boundaries, crystal imperfections or microporosity, which are not considered in the models, may result in dispersion of thermal waves and hence decrease the thermal diffusivity of our polycrystalline samples.

[29] Analysis of previous experimental data on thermal transport properties of mantle materials shows that thermal diffusivity values obtained on rocks or polycrystalline aggregates are generally lower than single crystal values. Measurements on polycrystalline samples are in good agreement with our data over a large range of temperatures (Table 3 and Figure 6). On the other hand, most olivine single-crystal data at ambient conditions are in relatively good agreement with the thermal diffusivity tensor used in the petrophysical models (Table 2). Anisotropy estimations in the present experiments are in good agreement with previous data for a dunite by *Kobayashi* [1974], which shows an anisotropy of 31% and 23% for thermal diffusivity and thermal conductivity measurements, respectively. This dunite has a similar olivine CPO to the one displayed by PNG [*Kasahara et al.*, 1968] for which 28.7% of thermal diffusivity anisotropy was predicted. Preservation of the anisotropy at high temperature in the present experiments is also in good agreement with data obtained on single crystals at high temperatures [*Kobayashi*, 1974], suggesting that thermal cracking, which is also anisotropic (most cracks are parallel to (010), since for olivine the [010] direction displays the highest thermal expansivity [*Bouhifd et al.*, 1996]), does not affect the evaluation of the anisotropy at high temperature. Thus the thermal diffusivity anisotropy measured at the rock scale is essentially due to the intrinsic thermal diffusivity anisotropy of its constituent minerals.

[30] In conclusion, the present study as well as previous data on mantle rocks highlights a discrepancy between the absolute values of thermal transport properties measured in single crystal and whole rocks at ambient conditions. This discrepancy may result from the large variety of methods used to measure thermal diffusivity/conductivity of single

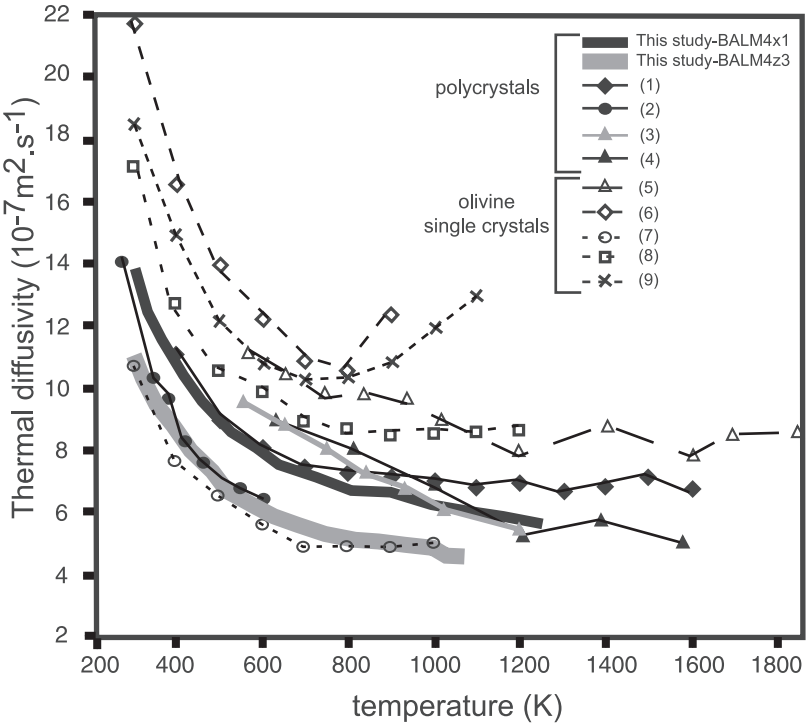

Figure 6. Comparison between thermal diffusivities obtained in the present study (BALM4 was chosen as the most representative sample) and a compilation of previous thermal diffusivity (or converted conductivity) measurements at high temperature. Open symbols/dashed lines represent measurements conducted on olivine single crystals, solid symbols/solid lines concern measurements performed on natural rocks or polycrystalline sintered aggregates, heavy solid lines show the present measurements (BALM4). References (indicated in parentheses in legend) are 1, *Katsura* [1995]; 2, *Beck et al.* [1978], Carolina dunite 1; 3, *Schatz and Simmons* [1972], Twin Sisters dunite; 4, *Schatz and Simmons* [1972], sintered forsterite; 5, *Schatz and Simmons* [1972], olivine single crystal [010] axis; 6, *Kobayashi* [1974], olivine single crystal −[100] axis; 7, *Kobayashi* [1974], olivine single crystal −[010] axis; 8, *Kobayashi* [1974], olivine single crystal −[001] axis; and 9, *Kanamori et al.* [1968], olivine single crystal −[001] axis.

crystals and polycrystalline samples. However, petrophysical models are able to predict the thermal diffusivity anisotropy of mantle rocks.

6. Temperature and Pressure Dependencies of the Thermal Diffusivity

6.1. Pressure Dependence

[31] Studies in a wide range of crystalline rocks show that after closure of microcracks, variation of thermal diffusivity with pressure is linear. This linear dependence on pressure is usually interpreted as an intrinsic effect of the pressure on the crystal structure of the rock-forming minerals. In order to compare the present results to previous studies, the rate of linear increase r is calculated by fitting each series of measurements for $P > 100$ MPa (Figure 5) by

$$D = D_0(1 + rP) \quad (2)$$

with pressure P in GPa.

[32] The parameters r obtained in the present study (5.5–13% GPa^{-1}) are in the same range than previous data for dunites and olivine single crystals at high pressure

Table 4. Rate of Linear Thermal Diffusivity Increase With Pressure at Room Temperature

Sample	Maximum Pressure, GPa	Calculated r, % GPa^{-1}	Ref[a]
Single crystal 1	4.95	8.1	3
San Carlos olivine Fo89	4.8	4	6
Sintered forsterite	5	18 (at 700 K)	1
Fo91 sintered aggregate	2	11	2
Fo89 sintered aggregate	9	4.9 (400 K)	5
Carolina dunite	4.95	5.2	3
Muskox dunite	4.95	4.7	3
Lherzolithe 4	1.2	11.9	4
BA2x1		13	
BA2z2		11.3	
VS24x2		8.1	
VS24z1	1	9.1	8
00BA1x1		5.5%	
00BA1z2		10.1%	
00VS11x1		11.2%	
Granites		12 ± 5%	7

[a]References: 1, *Fujisawa et al.* [1968]; 2, *Staudacher* [1973]; 3, *Beck et al.* [1978]; 4, *Horai and Susaki* [1989]; 5, *Katsura* [1995]; 6, *Zaug et al.* [1992]; 7, *Seipold* [1990]; and 8, this study.

Table 5. Photon Mean Free Path Length Estimates

Sample	Photon Mean Free Path Length	Ref[a]
Sintered forsterite, grain size = 15 μm	from 2 mm at 543 K to 1 mm at 1204 K	1
Twin sister dunite Fo94	from 0.9 mm at 554 K to 0.3 mm at 1200 K	1
Olivine single crystal Fo92	from 15 mm at 565 K to 1.7mm at 1215 K	1
Olivine single crystal Fo88	from 3.7 mm at 500 K to 1.49 mm at 1300 K	2

[a]References: 1, *Schatz and Simmons* [1972]; and 2, *Fukao et al.* [1968].

(Table 4). However, the present measurements on naturally deformed mantle rocks show a higher rate of increase of thermal diffusivity with pressure than theoretical calculations conducted for olivine ($r = 4\%$ GPa^{-1} [*Katsura*, 1995; *Hofmeister*, 1999]). Higher-pressure derivatives suggest that other processes than the compressibility of crystals affect the thermal diffusivity of our samples. In naturally deformed peridotites like the ones used in this study, micropores with an aspect ratio close to unity may remain open at high pressures (>100 MPa). Their closure at higher pressures may contribute to a higher rate r and to a scatter of r from sample to sample. Presence of micropores may also explain why the absolute values of thermal diffusivities are lower than the modeled ones, even at 1 GPa. Heterogeneity of void spaces or of the nonconnected porosity may also explain the observation that pressure derivative is dependent on the rock sample used, but independent of the measured direction (X or Z). This behavior is common in investigations of pressure dependence of thermal diffusivity or conductivity of crystalline rocks or sintered aggregates [*Seipold*, 1990, 2001].

6.2. Temperature Dependence

[33] Propagation of heat in dielectric solids is usually due to two different physical processes. The first is related to the vibrations of the atomic lattice, or, in a quantum mechanics point of view, to phonon propagation processes and is active over the entire temperature range. The second process concerns thermal radiation and interaction of photons with matter and operates at temperatures higher than 500K [*Schatz and Simmons*, 1972; *Shankland et al.*, 1979]. These two effects are responsible for the lattice diffusivity D_L and the radiative diffusivity D_R, respectively. Thus the thermal diffusivity $D(T)$ measured at a given temperature (T) is expected to be equal to

$$D(T) = D_L(T) + D_R(T). \quad (3)$$

In thermal diffusivity measurements under increasing temperature, the lattice contribution is usually well constrained [e.g., *Beck et al.*, 1978; *Holt*, 1975; *Kobayashi*, 1974]. The radiative heat transport is more difficult to measure because it depends strongly on the experimental conditions. An accurate measure of the radiative contribution to the total thermal diffusivity requires that radiative equilibrium must be reached during the experiments. This means that effective radiative diffusion processes through the sample will only be recorded if the heat transfer path is longer than the mean free path of photons. Moreover, the thermal gradient applied to the material must be as low as possible in order to have a nearly constant temperature over distances longer than the mean free path of photons, as expected in the mantle. If these conditions are not fulfilled, two opposite effects are predicted. First, the sample is not heated by the photonic heat transfer and its radiative diffusivity is not measured: the bulk diffusivity is underestimated [*Chui and Gardon*, 1969]. Second, the completely opaque thermocouple is directly heated by radiation and records an artificial increase of temperature, leading to an overestimation of the total thermal diffusivity. It is therefore impossible to interpret the measurement in terms of radiative transport.

[34] The distance over which heat transport is measured in our experiments (7 mm) is higher than the photon mean free path evaluated from previous data on a sintered forsterite aggregate (grain size 10 μm) or on a dunite [*Schatz and Simmons*, 1972] (Table 5). Photon mean free path measured in polycrystalline samples are significantly lower than the values obtained on single crystals (Table 5). Indeed, spectroscopic measurements conducted on olivine single crystals give an upper bound for the photon mean free path, since they measure the absorption of photons only within the single crystal [*Aronson et al.*, 1970; *Fukao et al.*, 1968; *Shankland et al.*, 1979] and do not evaluate the scattering of photons at grain boundaries, which is thought to reduce the photon mean free path [*Pitt and Tozer*, 1970]. Moreover, the higher iron content of the olivine in our samples (Table 1), compared to the sintered forsterite aggregate measured by *Schatz et al.* [1972], should increase the absorption and thus decrease the photon mean free path in our samples [*Burns*, 1970]. Our samples also contain pyroxenes, more absorbing than olivine, which may also reduce the photon mean free path. Finally, the amplitude of the temperature pulse imposed at the axis of the cylinder is low: the temperature elevation registered by the thermocouple is lower than 1.5 K. Thermal gradients within the sample are therefore minimized. In conclusion, the present experiments should be close to radiative equilibrium.

[35] In addition to the radiative equilibrium, chemical conditions prevailing during the experiments are also an important parameter. When an appropriate chemical buffer does not control oxygen fugacity, oxidation of Fe-bearing olivine at high temperature leads to formation of oxide films, characterized by a red coloration of the grains surface. Optical analysis of thin sections of heated samples shows that Fe-oxides films are developed along olivine grain or subgrain boundaries in all samples heated above 900 K. Development of these oxide films may be responsible for an increase in opacity of the samples and underestimation of radiative diffusivity. However, when the grain size is large (as in our samples 0.5–1 mm), probability of photon scattering at grain boundaries is low. Thus, if oxidation is restricted to grain boundaries only, it may not affect the radiative heat transport. Indeed, in *Schatz et al.*'s [1972] measurements, oxidation of the dunite sample is not ac-

companied by a strong decrease of the photon mean free path length.

6.2.1. Lattice Diffusivity

[36] Most theoretical and experimental studies on the temperature dependence of thermal diffusivity of rocks suggest that lattice diffusivity D_L is inversely proportional to the absolute temperature [*Klemens*, 1958; *Seipold*, 1998]. Indeed, the kinetic theory of gases, applied to a phonon gas, implies that

$$D_L = 1/3vl, \tag{4}$$

where v is the phonon velocity and l is the mean free path length of the phonons. As the phonon velocity, which is approximated by an average of the acoustic velocities over the three polarizations (Figure 2), is nearly constant with temperature (it decreases by <5% over 1000°C [*Isaak*, 1992]), the decrease of D_L with temperature is mainly due to the decrease of the phonon mean free path. Scattering of phonons by crystal imperfections limits the phonon mean free path, but it is assumed to be independent of temperature. On the other hand, phonon-phonon interactions related to the anharmonicity of lattice potential are strongly temperature dependent; they lead to a variation in 1/T of the phonon mean free path [*Klemens*, 1958]. In consequence, lattice diffusivity can be expressed as

$$D_L(T) = \frac{1}{A + BT}, \tag{5}$$

in which the parameter B quantifies the phonon-phonon interactions and the parameter A the interaction of phonons with crystal imperfections, such as point defects, dislocation wall, grain boundaries or microcracks [*Seipold*, 1998].

[37] However, it has been recently suggested that, although the thermal diffusivity or conductivity of simple solids such as periclase [e.g., *Katsura*, 1997] follow this law, the thermal conductivity of more complex substances, like silicates, should display a lower temperature dependence, following a T^{-a} law, where a is ~0.33 for silicates [*Hofmeister*, 1999]. This prediction is based on the assumption, often discussed [e.g., *Harrell et al.*, 2002; *Roufosse and Klemens*, 1974], that optic modes of phonons contribute with more than 50% to the total conductivity [*Hofmeister*, 1999]. As a consequence, a decreases as the number of optics modes of phonons increases, i.e., as the number of atoms per unit cell increases. On the basis of a calculation of phonons lifetimes, *Hofmeister* [1999] has proposed that the lattice conductivity K_L depends on temperature as

$$K_L(T) = K(298)\left(\frac{298}{T}\right)^a \exp\left(-\left(4\gamma_{Th} + \frac{1}{3}\right)\int_{298}^{T} \alpha(T)dT\right), \tag{6}$$

where γ_{th} is the thermal Grüneisen parameter, taken as equal to 1.2, and $\alpha(T)$ is the thermal expansion.

[38] The lattice diffusivity is obtained by dividing equation (6) by the term $\rho(T)C_p(T)$:

$$D_L(T) = \frac{K_L(T)}{\rho(T)C_P(T)}, \tag{7}$$

where $\rho(T)$ is the density, $C_P(T)$ is the heat capacity at constant pressure.

[39] These two laws (equations (5) and (6)) imply a zero value of the lattice thermal diffusivity at infinite temperature. As pointed by *Slack* [1979], lattice thermal diffusivity in a dielectric solid has a positive lower bound different from zero, since the phonon mean free path (equation (4)) cannot be smaller than a small multiple of the interatomic distance [*Harrell et al.*, 2002]. Nevertheless, these laws are assumed to describe correctly the behavior of the rocks if the lower limit of the phonon mean free path is not reached in the studied temperature. This lower limit is expected to be reached at temperatures close to the melting point of the material [*Slack*, 1979; *Roufosse and Klemens*, 1973, 1974]. Thus, for the studied temperature range (<1000°C), the two proposed temperature dependencies may correctly describe the observed temperature dependence of the lattice thermal diffusivity of peridotites.

[40] In order to bound the lattice diffusivity measured in this study, data are fitted at temperatures <520 K, for which the radiative diffusivity is assumed to be negligible, by equation (5) (taken as a lower bound) and equations (6) and (7) (taken as an upper bound) (Figure 7). A Levenberg-Marquardt algorithm that minimizes the chi-square coefficient is used. Fitting parameters and associated mean squared errors are calculated separately for each measurement direction (Table 6). The two fits are equally good at low temperatures. The a parameters obtained are in good agreement with *Hofmeister*'s [1999] predictions for silicates. The parameters A and B are in good agreement with previous studies on peridotites [*Seipold*, 1998]. The main difference between the two fits appears in the extrapolation of calculated lattice diffusivity to high temperatures (Figure 7).

[41] Analysis of these fitting coefficients is important in order to evaluate the processes of phononic transport, especially anisotropy. Calculated phonon velocities of the studied samples show a weak anisotropy, between 3.4 and 6.1% (Figure 2). Thus the anisotropy of lattice thermal diffusivity is mainly due to an anisotropy of the phonon mean free path length, which must be maximum parallel to the [100] axis of olivine (equation (4)). At the rock scale, this anisotropy may be due to (1) a lower density of crystalline imperfections parallel to the [100] direction or (2) phonon-phonon interactions. In the first case the coefficient A (equation (5)) should be higher parallel to the [100] direction, while in the second case the temperature dependence, which is characterized by the parameters B (equation (5)) or a (equation (6)), should be lower parallel to the [100] direction. The parameter A varies slightly from sample to sample, and does not display a systematic variation as a function of the structural direction (Table 6). On the other hand, the B and a parameters are systematically lower in measurements parallel to the X direction (Table 6); this accounts for the preservation of the thermal diffusivity anisotropy at high temperature. Therefore phonon-phonon interactions resulting from the anharmonic properties of the olivine lattice control the anisotropy of thermal diffusivity. This conclusion is in agreement with the prediction of the anisotropy of thermal diffusivity at room temperature using a space-dependent Grüneisen parameter, which quantifies the anharmonic properties of a crystallographic lattice [*Chai et al.*, 1996]. The present result confirms that the anisotropy

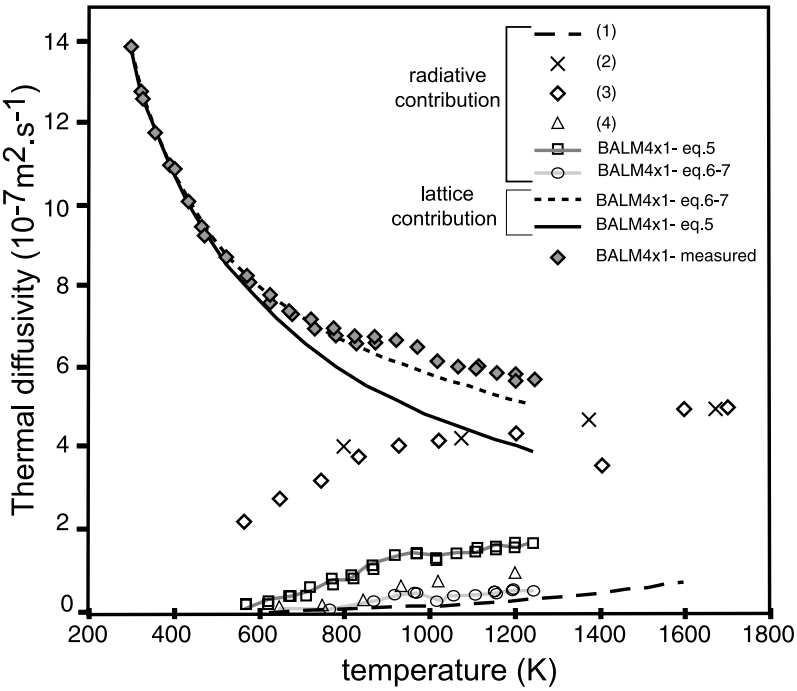

Figure 7. Lattice thermal diffusivity calculated by fitting the measured diffusivity of sample BALM4x1 up to 520 K by equation (5) (dashed line) and equations (6) and (7) (solid line). Radiative components (open squares and circles) were obtained by extrapolating the calculated lattice diffusivity to higher temperatures and evaluating the difference between the measured total diffusivity and the calculated lattice diffusivity. Previous estimates of radiative thermal diffusivity for olivine single crystals and olivine aggregates obtained from spectroscopic determinations [*Shankland et al.*, 1979], modified Angstrom method [*Schatz and Simmons*, 1972] and infrared reflectivity spectroscopy [*Hofmeister*, 1999] are presented for comparison. References (indicated in parentheses in legend) are 1, *Hofmeister* [1999]; 2, *Shankland et al.* [1979]; 3, *Schatz and Simmons* [1972], olivine single crystal; and 4, *Schatz and Simmons* [1972], dunite.

of thermal diffusivity observed at the rock scale is essentially controlled by the intrinsic properties of olivine crystals and by the deformation-induced crystal preferred orientations of this mineral.

6.2.2. Radiative Contribution

[42] The heat transfer by photons D_R is usually approximated by the following law:

$$D_R = \frac{16\sigma n^2 T^3}{3\rho C_P} l_R(T), \tag{8}$$

where σ is the Stefan-Boltzmann constant, n is the refractive index, and l_R is the photon mean free path length, which is equal to the inverse of the absorption coefficient and varies with temperature. If the difference between the measured diffusivity and the extrapolated lattice diffusivity represents the radiative diffusivity, it appears that *Hofmeister*'s [1999] approach (equations (6) and (7)) applied to the present results implies that the contribution of the radiative transport to thermal diffusivity is negligible compared to the lattice diffusivity (<10% at 1250 K). According to equation (8), this low contribution of radiative heat transport indicates that the constitutive minerals of these samples absorb most thermal radiation and that extrapolation of thermal diffusivity values to higher temperatures conditions is weakly affected by radiative transport, in spite of the strong temperature dependence of the latter. If the radiative

Table 6. Estimated Fitting Parameters for the Lattice Diffusivity up to 520 K Using Equation (5) for A and B and Equations (6) and (7) for a[a]

Data	A, 10^5 m^{-2} s	B, 10^3 m^{-2} s K^{-1}	a
Average in the X direction	1.52±0.3 (0.11)	1.9±0.07 (0.11)	0.31±0.004 (0.04)
Average in the Y direction	1.1±0.2 (0.09)	2.23±0.05 (0.09)	0.37± 0.01 (0.02)
Average in the Z direction	1.33±0.1 (0.07)	2.45±0.1 (0.07)	0.36±0.02 (0.08)
BALM4x1 (representative sample)	1.16 (0.139)	1.92 (0.139)	0.317 (0.036)

[a]These parameters represent an average over all measurements of this study, in each direction, with standard deviation. Values in parentheses are the average mean squared error associated with each fit. Also shown are the fitting parameters of BALM4x1, chosen as the most representative sample.

diffusivity is evaluated from the lattice diffusivity calculated in equation (5), the radiative heat transport accounts for 30% of the total diffusivity at 1250 K and its contribution has to be considered when extrapolating thermal diffusivity values to higher temperatures. Additional independent measurements of lattice or radiative contributions are required to discriminate these two models.

[43] The radiative diffusivities estimated in the present experiments using the two models bound the radiative diffusivity measured in a dunite by *Schatz and Simmons* [1972] (Figure 7), where radiative equilibrium was expected due to the length of the sample (~10 mm). The higher thermal diffusivity values observed by *Katsura* [1995] experiments at temperatures >1000 K may be due to the small samples used, which did not allow thermal equilibrium (Figure 6). The discrepancy between the present results and previous data on single crystals at high temperature is higher, but it is mainly correlated to the difference on thermal diffusivity estimations at ambient conditions (discussed previously). However, some data show a strong increase of the total diffusivity at high temperature, suggesting a strong radiative contribution [*Kanamori et al.*, 1968] (Figure 6), but the small samples used in this study may have hindered the radiative equilibrium. On the other hand, other studies display a flattening of the total thermal diffusivity curve, suggesting a lower radiative contribution, in agreement with a decrease of the photon mean free path with temperature [*Schatz and Simmons*, 1972]. Finally, calculations based on optical absorption spectra of olivine suggest a strong radiative contribution [*Fukao et al.*, 1968; *Shankland et al.*, 1979], in disagreement with the total thermal diffusivity measured in the present experiments (Figure 7). However, the low-temperature derivatives of the radiative diffusivity deduced from these spectroscopic experiments are in agreement with our measurements (Figure 7), which confirms that the absorption coefficient of olivine increases strongly at high temperature (equation (8)).

7. Conclusion

[44] Numerical modeling of the three dimensional distribution of the thermal diffusivity of seven peridotites rocks suggests that the crystal preferred orientation of olivine formed by solid-state flow in the upper mantle induces a strong anisotropy of thermal diffusivity. Thermal diffusivity is up to 25% higher parallel to the flow direction (i.e., parallel to the olivine [100] axes concentration) than normal to the foliation plane (i.e., parallel to the [010] axes concentration). Measurements of the thermal diffusivity of these peridotites under increasing pressure and temperature show that this anisotropy is preserved at the rock scale under high–temperature and high-pressure conditions. Analysis of the temperature and pressure dependencies of thermal diffusivity confirms that the anisotropy observed at the rock scale is essentially controlled by the intrinsic properties of the olivine crystal and by the deformation-induced crystal preferred orientation of this mineral.Minimization of radiative disequilibrium in the present experiments allows the measurement of the total thermal diffusivity. We used two different lattice diffusivity models to estimate the radiative contribution at high temperature. In both cases, the radiative contribution is lower than suggested by spectroscopic data on olivine single crystals. However, extrapolation of the present data to higher temperature conditions depends on the model: the radiative contribution to heat transport is important if the lattice contribution is inversely dependent on temperature, but it may be negligible if optic modes of phonons contribute significantly to heat transfer at high temperature.

[45] Although the measured anisotropies are consistent with the predictions of the petrophysical models (15–25% of anisotropy), measured thermal diffusivities are 20–30% lower than model predictions. This discrepancy between measurements and model predictions cannot be explained by the presence of cracks in the samples because the closure of these void spaces, evaluated through the high-pressure experiments, is found to have a negligible effect on measured thermal diffusivities. Previous data on mantle rocks also highlight a discrepancy between single crystal and whole rock thermal transport properties at ambient conditions. This suggests that the discrepancy may result from the large variety of methods used to measure thermal diffusivity/conductivity of single crystals and polycrystalline samples.

[46] Deformation-induced olivine crystal preferred orientations in the upper mantle results in both an anisotropic heat transfer and seismic wave propagation. Measurements of seismic anisotropy, such as shear wave splitting, imply that deformation-induced olivine preferred orientations are consistent at large scales (>50 km) in the upper mantle. Thus heat transport in the upper mantle should be anisotropic at these scales. A thermal anomaly should propagate faster parallel to the olivine [100] preferred orientation, i.e., parallel to the fast *S* wave polarization direction (or the fastest *P* wave velocity direction) and slower parallel to the xolivine [010] preferred orientation, i.e., parallel to the slowest *P* wave velocity direction. Since the upper mantle rheology is strongly temperature-dependent, faster heat transport parallel to the flow direction, to which is associated the preferred orientations of olivine [100] axes in the upper mantle, may induce localization of deformation. Within the lithospheric mantle, it may add to a CPO-induced mechanical anisotropy [*Tommasi and Vauchez*, 2001] to favor the reactivation of preexisting structures.

[47] **Acknowledgments.** We thank J. M. Brown and W. B. Durham for their constructive reviews. We thank Cornelia Karger and Rainer Becker for their participation in the measurements and Christophe Nevado for the high-quality polished thin sections. Matteo Ferrero (Nuova Cives S.R.L.) and Françoise Boudier are thanked for providing the samples from Baldissero and Papua New Guinea, respectively. The Laboratoire de Tectonophysique's EBSD system was funded by the CNRS/INSU, Université of Montpellier II, and NSF project "Anatomy of an Archean craton". This work was supported by the CNRS/INSU program "Action Thématique Innovante".

References

Abramson, E. H., J. M. Brown, L. J. Slutsky, and J. Zaug, The elastic constants of San Carlos olivine to 17 GPa, *J. Geophys. Res.*, *102*(B6), 12,253–12,263, 1997.

Aronson, J. R., L. H. Belloti, S. W. Eckroad, A. G. Emslie, R. K. McConnell, and P. C. Von Thuna, Infrared spectra and radiative thermal conductivity of minerals at high temperatures, *J. Geophys. Res.*, *75*(17), 3443–3456, 1970.

Beck, A. E., D. M. Darbha, and H. H. Schloessin, Lattice conductivities of single-crystal and polycrystalline materials at mantle pressures and temperatures, *Phys. Earth Planet. Inter.*, *17*, 35–53, 1978.

Bouhifd, M. A., D. Andrault, G. Fiquet, and P. Richet, Thermal expansion of forsterite up to the melting point, *Geophys. Res. Lett.*, *23*(10), 1143–1146, 1996.

Bunge, H. J., *Texture Analysis in Materials Sciences*, 593 pp., Butterworths, London, 1982.

Burns, R. G., *Mineralogical Application of Crystal Field Theory*, Cambridge Univ. Press, New York, 1970.

Carslaw, N. S., and J. C. Jaeger, *Conduction of Heat in Solids*, Oxford Univ. Press, New York, 1959.

Chai, M., J. M. Brown, and L. J. Slutsky, Thermal diffusivity of mantle minerals, *Phys. Chem. Miner.*, *23*, 470–475, 1996.

Chui, G. K., and R. Gardon, Interaction of radiation and conduction in glass, *J. Am. Ceram. Soc.*, *52*(10), 548–553, 1969.

Duffy, T. S., and M. T. Vaughan, Elasticity of enstatite and its relationships to crystal structure, *J. Geophys. Res.*, *93*(B1), 383–391, 1988.

Durham, W. B., V. V. Mirkovich, and H. C. Heard, Thermal diffusivity of igneous rocks at elevated pressure and temperature, *J. Geophys. Res.*, *92*(B11), 11,615–11,634, 1987.

Fujisawa, H., N. Fujii, H. Mizutani, H. Kanamori, and S. Akimoto, Thermal diffusivity of Mg_2SiO_4, Fe_2SiO_4, and NaCl at high pressures and temperatures, *J. Geophys. Res.*, *73*(14), 4727–4733, 1968.

Fukao, Y., H. Mizutani, and S. Uyeda, Optical absorption spectra at high temperatures and radiative thermal conductivity of olivines, *Phys. Earth Planet. Inter.*, *1*, 57–62, 1968.

Harrell, M., J. M. Brown, and E. H. Abramson, Anisotropic lattice thermal conductivity of upper mantle minerals at high temperature, *Eos Trans. AGU*, *83*(47), Fall Meet. Suppl., Abstract MR11A-13, 2002.

Hofmeister, A. M., Mantle values of thermal conductivity and the geotherm from phonon lifetimes, *Science*, *283*, 1699–1706, 1999.

Holt, J. B., Thermal diffusivity of olivine, *Earth Planet. Sci. Lett.*, *27*, 404–408, 1975.

Horai, K., Thermal conductivity of rock-forming minerals, *J. Geophys. Res.*, *76*(5), 1278–1308, 1971.

Horai, K., and J. Susaki, The effect of pressure on the thermal conductivity of silicate rocks up to 12 kbar, *Phys. Earth Planet. Inter.*, *55*, 292–305, 1989.

Isaak, D. G., temperature elasticity of iron-bearing olivines, *J. Geophys. Res.*, *97*(B2), 1871–1885, 1992.

Kanamori, H., N. Fujii, and H. Mizutani, Thermal diffusivity measurement of rock-forming minerals from 300°K to 1100°K, *J. Geophys. Res.*, *73*(2), 595–605, 1968.

Kasahara, J., I. Suzuki, M. Kumazawa, Y. Kobayashi, and K. Iida, Anisotropism of *P* wave in dunite, *J. Seismol. Soc. Jpn.*, *21*, 222–228, 1968.

Katsura, T., Thermal diffusivity of olivine under upper mantle conditions, *Geophys. J. Int.*, *122*, 63–69, 1995.

Katsura, T., Thermal diffusivity of periclase at high temperatures and high pressures, *Phys. Earth Planet. Inter.*, *101*, 73–77, 1997.

Klemens, P. G., Thermal conductivity and lattice vibrational modes, *Solid State Phys.*, *7*, 1–98, 1958.

Kobayashi, Y., Anisotropy of thermal diffusivity in olivine, pyroxene, and dunite, *J. Phys. Earth*, *22*, 359–373, 1974.

Kukkonen, I. T., J. Jokinen, and U. Seipold, Temperature and pressure dependencies of thermal transport properties of rocks: Implications for uncertainties in thermal lithosphere models and new laboratory measurements of high-grade rocks in the central fennoscandian shield, *Surv. Geophys.*, *20*, 33–59, 1999.

Mainprice, D., and M. Humbert, Methods of calculating petrophysical properties from lattice preferred orientation data, *Surv. Geophys.*, *15*, 575–592, 1994.

Pitt, G. D., and D. C. Tozer, Radiative heat transfer in dense media and its magnitude in olivines and some other ferromagnesian minerals under typical upper mantle conditions, *Phys. Earth Planet. Inter.*, *2*, 189–199, 1970.

Pribnow, D., and T. Umsonst, Estimation of thermal conductivity from mineral composition: Influence of fabric and anisotropy, *Geophys. Res. Lett.*, *20*(20), 2199–2202, 1993.

Roufosse, M., and P. G. Klemens, Thermal conductivity of complex dielectric crystals, *Phys. Rev. B*, *7*, 5379–5386, 1973.

Roufosse, M., and P. G. Klemens, Lattice thermal conductivity of minerals at high temperatures, *J. Geophys. Res.*, *79*(5), 703–705, 1974.

Schatz, J. F., and G. Simmons, Thermal conductivity of earth materials at high temperatures, *J. Geophys. Res.*, *77*(35), 6966–6983, 1972.

Seipold, U., Simultaneous measurements of thermal diffusivity and thermal conductivity under high pressure using thermal pulse of finite length, *High Temp. High Pressures*, *20*, 609–613, 1988.

Seipold, U., Pressure and temperature dependence of thermal transport properties for granites, *High Temp. High Pressures*, *22*, 541–548, 1990.

Seipold, U., Temperature dependence of thermal transport properties of crystalline rocks—A general law, *Tectonophysics*, *291*, 161–171, 1998.

Seipold, U., Der warmetransport in kristallinen gesteien unter den bedingungen der kontinentalen cruste, *Sci., Tech. Rep. STR01/13*, GeoForschungsZentrum Potsdam, Potsdam, Germany, 2001.

Seipold, U., H.-J. Mueller, and P. Tuisku, Principle differences in the pressure dependence of thermal and elastic properties of crystalline rocks, *Phys. Chem. Earth*, *23*(3), 357–360, 1998.

Shankland, T. J., U. Nitsan, and A. G. Duba, Optical absorption and radiative heat transport in olivine at high temperature, *J. Geophys. Res.*, *84*(B4), 1603–1610, 1979.

Siegesmund, S., Modelling the thermal conductivity observed in paragneisses of the KTB pilot hole, *Sci. Drill.*, *4*, 207–213, 1994.

Slack, G. A., The thermal conductivity of nonmetallic crystals, *Solid State Phys.*, *34*, 1–71, 1979.

Staudacher, W., Die Temperatur-Leitfähigkeit von natürlichem olivin bei hohen drucken und temperatur, *Z. Geophys.*, *39*, 979–988, 1973.

Taylor, R., Thermal diffusivity of composites, *High Temp. High Pressures*, *15*, 299–309, 1983.

Tommasi, A., and A. Vauchez, Continental rifting parallel to ancient collisional belts: An effect of the mechanical anisotropy of the lithospheric mantle, *Earth Planet. Sci. Lett.*, *185*, 199–210, 2001.

Tommasi, A., B. Tikoff, and A. Vauchez, Upper mantle tectonics: Three-dimensional deformation, olivine crystallographic fabrics and seismic properties, *Earth Planet. Sci. Lett.*, *168*, 173–186, 1999.

Tommasi, A., B. Gibert, U. Seipold, and D. Mainprice, Anisotropy of thermal diffusivity in the upper mantle, *Nature*, *411*, 783–786, 2001.

Zaug, J., J. M. Abramson, J. M. Brown, and L. J. Slutsky, Elastic constants, equation of state and thermal diffusivity at high pressure, in *High-Pressure Research: Applications to Earth and Planetary Sciences*, edited by Y. Syono and M. H. Manghani, pp. 157–166, Terra Sci., Tokyo, 1992.

B. Gibert, D. Mainprice, and A. Tommasi, Laboratoire de Tectonophysique, Université Montpellier II and CNRS, Place Eugène Bataillon, F-34095 Montpellier cedex 5, France. (gibert@dstu.univ-montp2.fr)

U. Seipold, GeoForschungsZentrum Potsdam, Division 5, Telegrafenberg, D-14473 Potsdam, Germany.